

## Supporting Information

### **Glycol ether additives control the size of PbS nanocrystals at reaction completion**

Philippe B. Green<sup>a</sup>, Zhibo Wang<sup>b</sup>, Philip Sohn<sup>a</sup>, Christian J. Imperiale<sup>a</sup>, Oleksandr Voznyy<sup>b</sup>, and Mark W.B. Wilson<sup>a</sup>

<sup>a</sup> Department of Chemistry, University of Toronto, Toronto, Ontario M5S3H6, Canada

<sup>b</sup> Department of Physical and Environmental Science, University of Toronto Scarborough, Toronto, Ontario M1C 1A4, Canada

### **Materials**

Lead (II) Oxide (Sigma Aldrich 99.999%), Hexamethyldisilathiane (TMS-S, Sigma Aldrich), Oleic Acid (OA, Sigma Aldrich 90%), 1-Octadecene (ODE, Sigma Aldrich 90%), Diglyme (Sigma Aldrich, 99.5%), Triglyme (Sigma Aldrich, 99%), Tetraglyme (Sigma Aldrich, 99%), Acetone (Sigma Aldrich 99.6%), Tetrachloroethylene (TCE, Sigma Aldrich 90%), Hexanes (Sigma Aldrich 99%) were used without further purification.

### **PbS Nanocrystal Synthesis:**

(6:1 OA:Pb, 0.14:1 S:Pb in 25 mL of ODE):

The reaction was performed similarly to our previous publication,<sup>1</sup> with the primary difference being the addition of glycol ethers. This method was in turn adapted from the method of Lee et al<sup>2</sup>. In brief, the Lee reaction derives from the conventional reaction developed by Hines and Scholes,<sup>3</sup> but is more dilute and uses additional equivalents of OA. For complete reactions, the lead solution was prepared by adding 0.223g (1 mmol) of lead oxide, 1.9 mL OA (1.7g, 6 mmol) and 25 mL ODE in a three-neck round-bottom flask. The solution was placed under vacuum, heated to 120<sup>o</sup>C, and vigorously stirred until all the lead oxide dissolved. Solutions turned pale yellow. The solution was then set to the desired temperature and left to stabilize. The TMS-S solution was prepared by adding 0.03 mL (0.14 mmol) of TMS-S to 1.5 mL of ODE in a nitrogen glovebox and then loading the mixture into a syringe. Once the desired temperature of the lead solution was reached, the TMS-S solution was rapidly injected. The solution changed color, turning from red to black in the colder reactions while going immediately to black in hotter reactions. 0.2 mL aliquots were periodically collected and crashed with 0.4 mL of acetone and centrifuged for 40s at 6000 rpm (4430 rcf). The precipitate was then re-dissolved in 0.2 mL TCE. Any further variations in temperatures, OA:Pb, S:Pb, and concentrations from these conditions are explicitly noted.

The addition of the glycol ethers (diglyme, triglyme, or tetraglyme) was performed after the solution reached 90<sup>o</sup>C. This cooled the solution; thus, the solution was then reheated to 90<sup>o</sup>C and left to settle for 5 minutes. The addition of glycol ethers produced no visible appearance change to the Pb solution. After the injection of TMS-S, the effect of the glycol ethers can be visually observed as the reaction progresses from clear to red to black considerably faster.

**Lead oleate (Pb(Oleate)<sub>2</sub>) synthesis:**

(2.02:1 OA:Pb, in 25 mL of Toluene):

Lead oleate was synthesized by mixing 0.223g of PbO and 0.64 mL of oleic acid in 25 mL of toluene. The solution was heated to 110°C in an oil bath until the solid PbO dissolved completely. The toluene was then evaporated using an air aspirator. Samples with glycol ethers were prepared in a similar way (25 GE:Pb), but were subsequently vacuum-filtrated and washed with toluene. This yielding white free-flowing powders used for the <sup>1</sup>H NMR measurements.

**Relation between reaction completion and synthetic yield:**

We adopt a convention from the colloidal nanocrystal literature<sup>4</sup> and define that completion is reached when nanocrystal growth reaches its asymptote in a given reaction. With PbS NCs, this can be observed spectroscopically when the excitonic absorption/emission peaks cease red-shifting (e.g. Figure 2). Alternatively, completion can be assessed by monitoring the strength of the optical absorption at  $\lambda$ : 400nm, because is proportional to the total number of PbS equivalents within the nanocrystals.<sup>5</sup> Figures S17 and S19 present the optical absorption of aliquots taken periodically during a typical PbS NCs, and show that these two spectroscopic observables reach their asymptotic values co-incidently in our reactions.

It has been previously shown that completion, as defined above, commonly co-incides with exhaustion of the limiting reagent (*i.e.* sulfur), and synthetic yields above 80%.<sup>6-8</sup> We expect comparable behaviour from the reactions in this paper, though we did not explicitly quantify the synthetic yield—despite observing <sup>1</sup>H NMR signals in the post-reaction mixture consistent with a residual concentration glycol ethers chelated to Pb(Oleate)<sub>2</sub> (S3-S7). This is because our reactions are performed with a large Pb excess (>6:1) because these conditions were previously shown to yield PbS NCs with the narrowest ensemble linewidths for the size range considered.<sup>1,9</sup>

**Characterization:**

Optical absorption spectra were taken on a Cary 5000 UV-vis-NIR spectrophotometer or a Perkin Elmer Lambda 1050 UV/Vis spectrophotometer. Emission spectra were obtained upon laser excitation at  $\lambda$ =450 nm using fiber-coupled Flame (500 nm <  $\lambda$  < 1000 nm) or NIRQuest ( $\lambda$  > 920 nm) spectrometers (Ocean Optics). NMR spectroscopy was performed on a 300 MHz Varian MercuryPlus NMR spectrometer. Toluene d8 was used as the solvent.

Table S1:

	Coupled	Uncoupled	Delta (Ha)	Delta (eV)	Delta (Kcal/mol)
Diglyme	-225.853	-225.823	0.029973	<b>0.81</b>	<b>18.679</b>
Triglyme	-255.624	-255.589	0.035438	<b>0.96</b>	<b>22.138</b>
Tetraglyme	-285.398	-285.353	0.04496	<b>1.22</b>	<b>28.134</b>

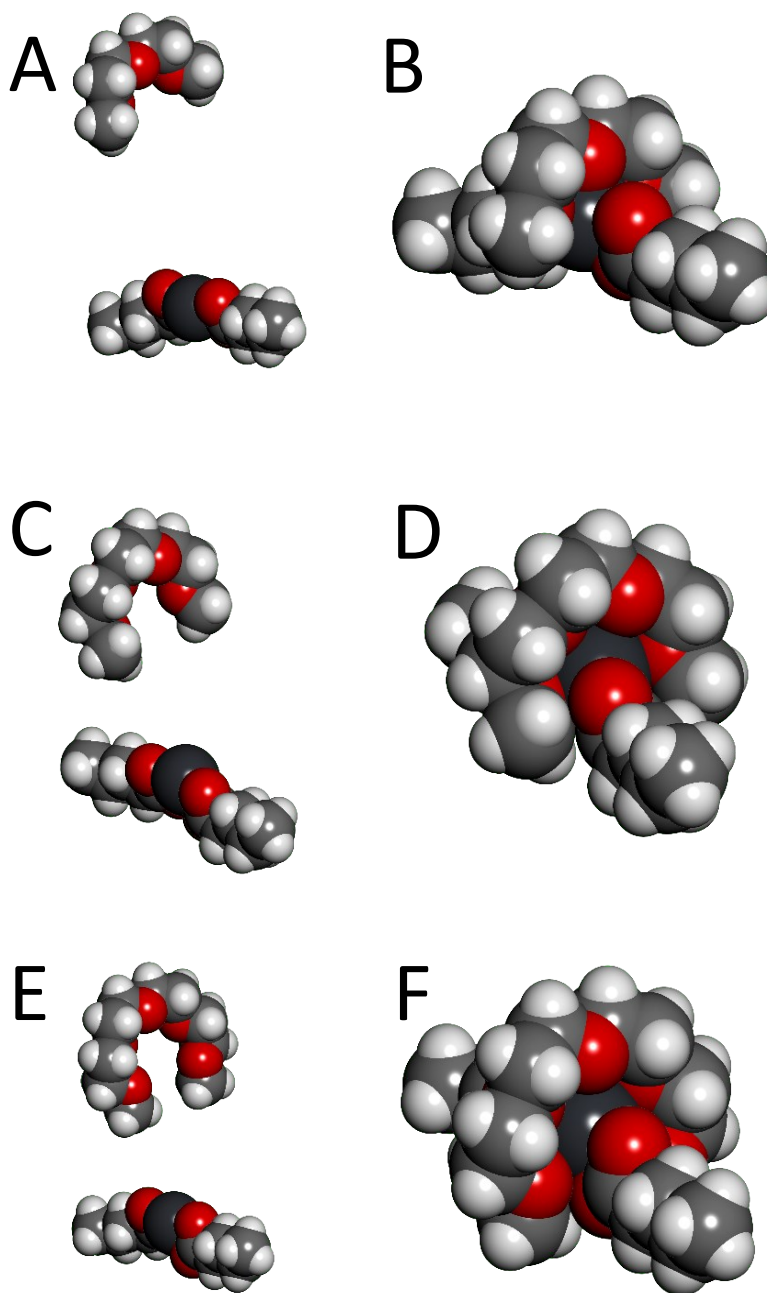


Figure S1: Relaxed geometries of coupled and uncoupled glycol ethers and lead butyrate. A, B) Diglyme, C, D) triglyme and E, F) tetraglyme. The non-polar, non-co-ordinating solvent used in synthesis (1-octadecene) was ignored in these simulations. As can be observed, all three glycol ethers are able wrap around the Pb atom to form a stable complex.

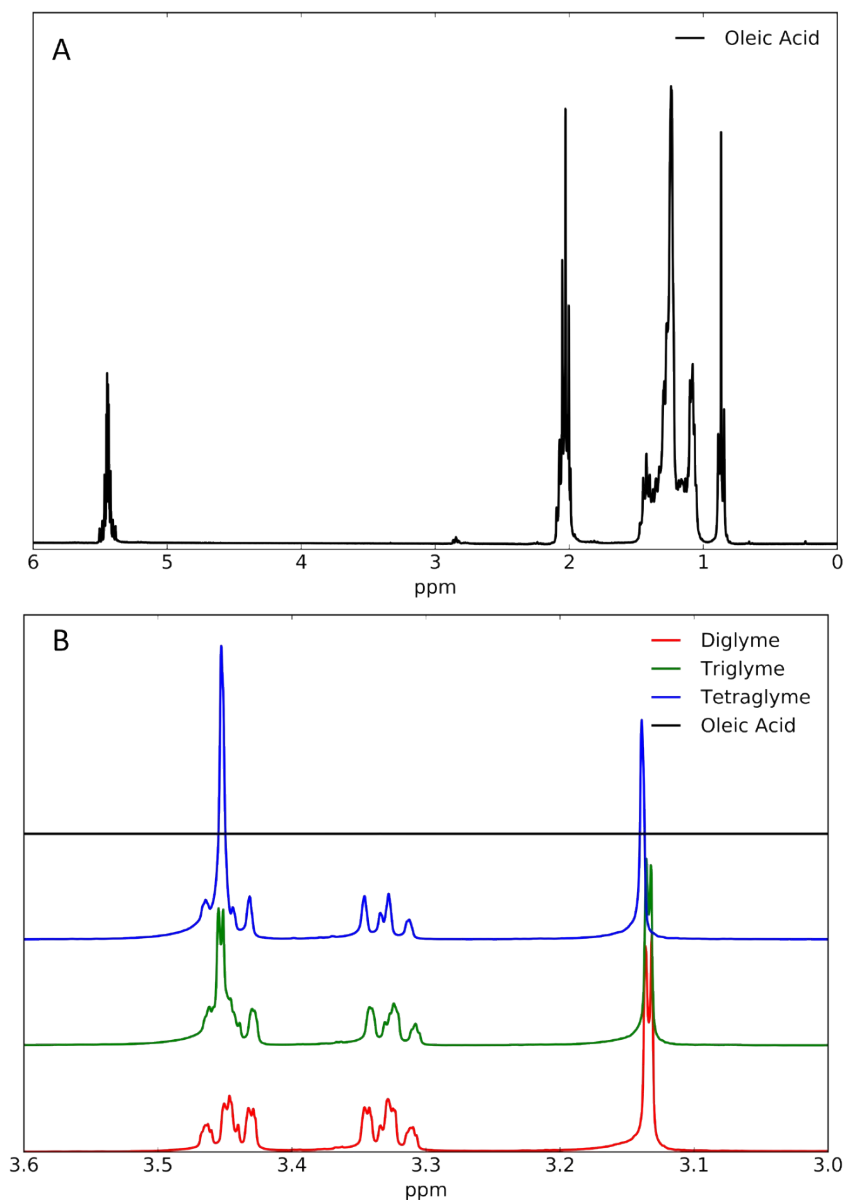


Figure S2: <sup>1</sup>H NMR of oleic acid (A) and the three glycol ethers (B) used in this study. Peaks are consistent with expectations from the molecular structures (Figure 1A), and do not overlap. This allows the two reagents used in a particular synthesis (*i.e.* (OA and one glycol ether) to be distinguished.

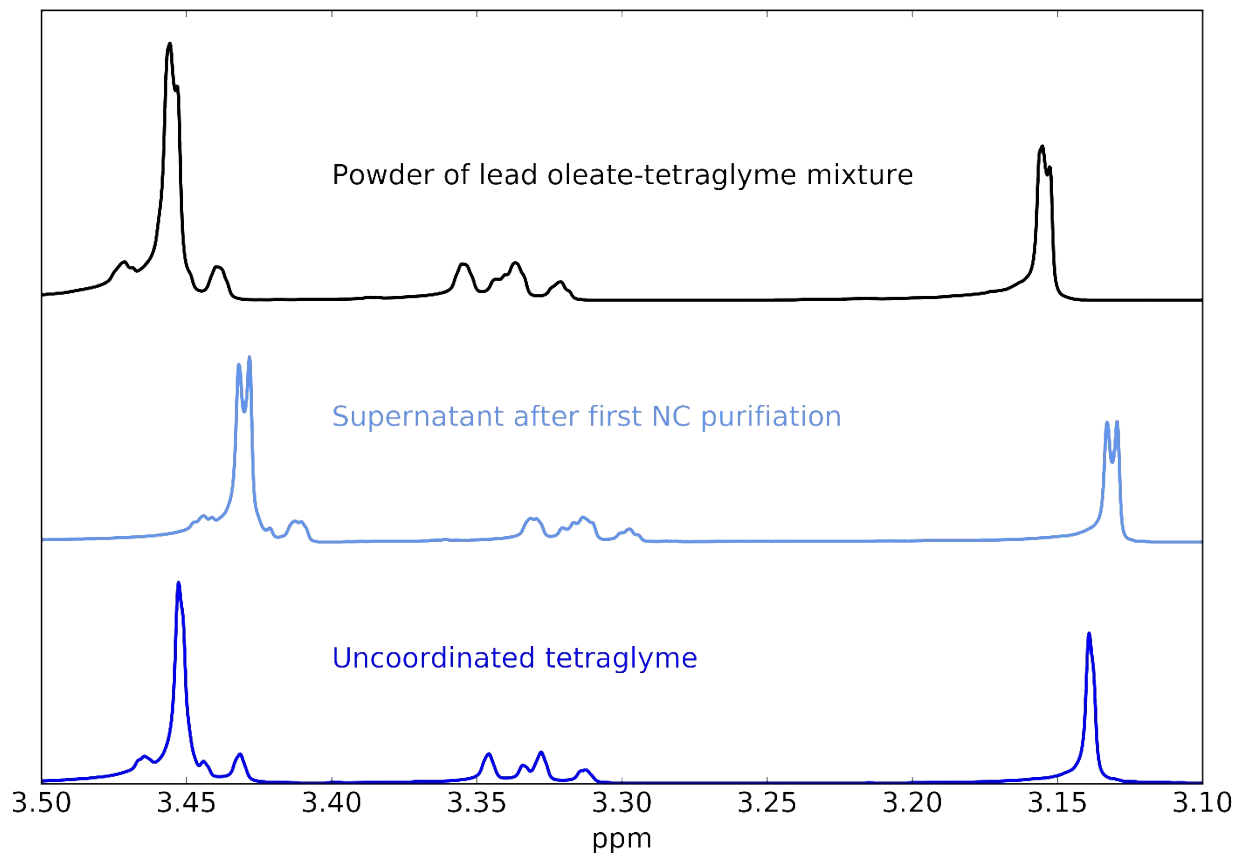


Figure S3: <sup>1</sup>H NMR spectra of uncoordinated tetraglyme, residual tetraglyme in the supernatant following PbS synthesis and purification, and a powder containing an independently synthesized mixture of Pb(oleate)<sub>2</sub> and tetraglyme (see Methods). Both spectra extracted in the presence of Pb show a new splitting of the <sup>1</sup>H resonances. This evidence of an altered chemical environment is consistent with reduced conformational flexibility resulting from the co-ordination of tetraglyme to lead oleate.

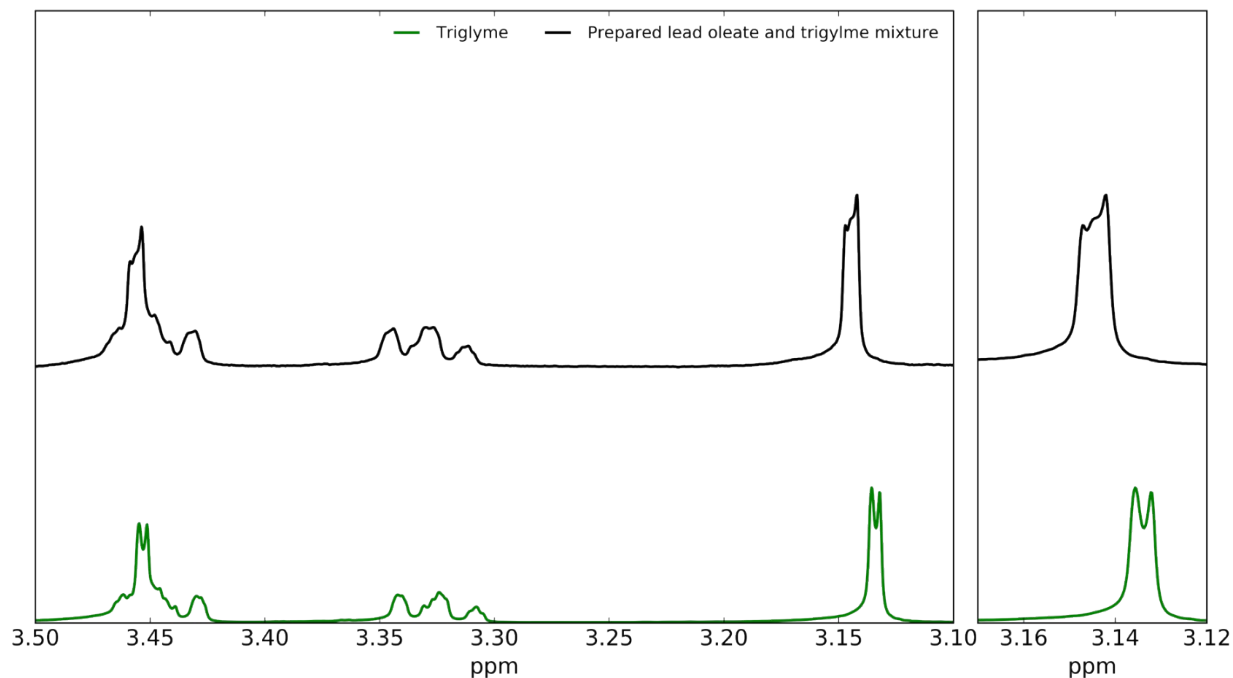


Figure S4: NMR spectra of uncoordinated triglyme and a powder containing a lead oleate triglyme mixture (See Methods). The lead oleate powder prepared with triglyme yields a further splitting of the  $^1\text{H}$  resonances, with the two-peaked resonances at approximately 3.45 and 3.13 ppm (the latter highlighted in the expanded scale at right) becoming three-peaked. Similar to our observations with tetraglyme, this is consistent with co-ordination to lead oleate.

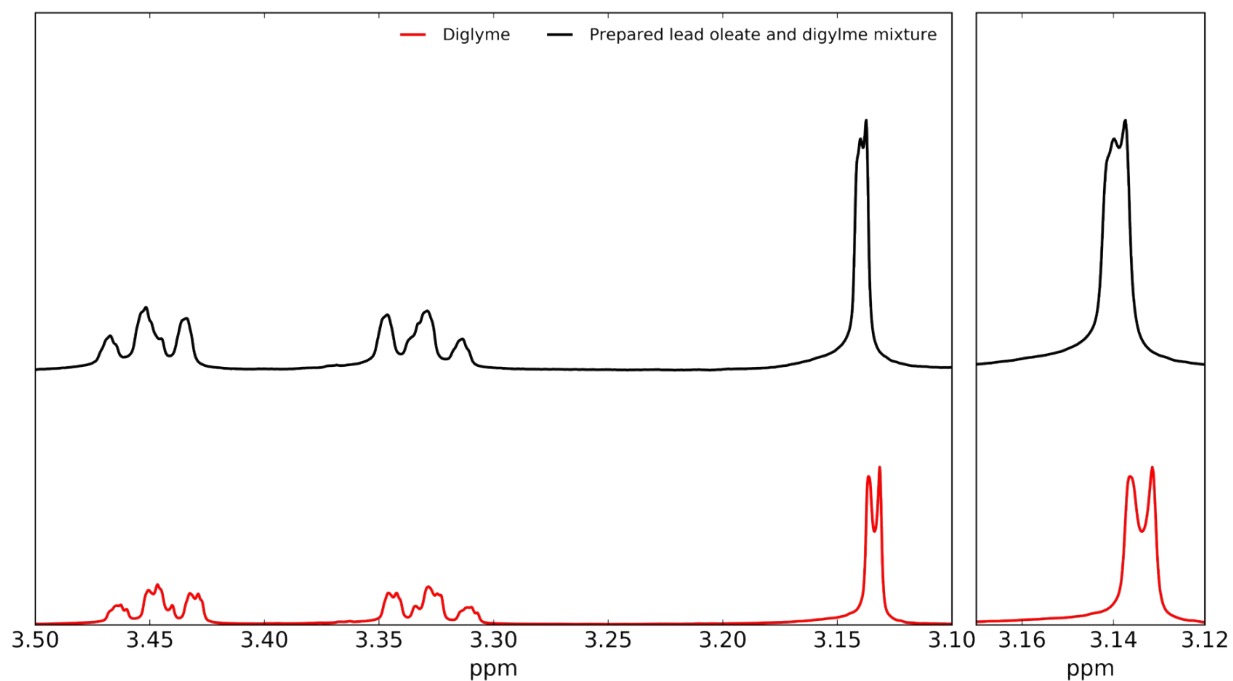


Figure S5: NMR spectra of uncoordinated diglyme and a powder containing a lead oleate diglyme mixture (See Methods). The powder yields a further splitting of the  $^1\text{H}$  resonance at approximately 3.13 ppm (highlighted in the expanded scale at right) becoming three-peaked. Similar to our observations with tetraglyme, this is consistent with co-ordination to lead oleate.

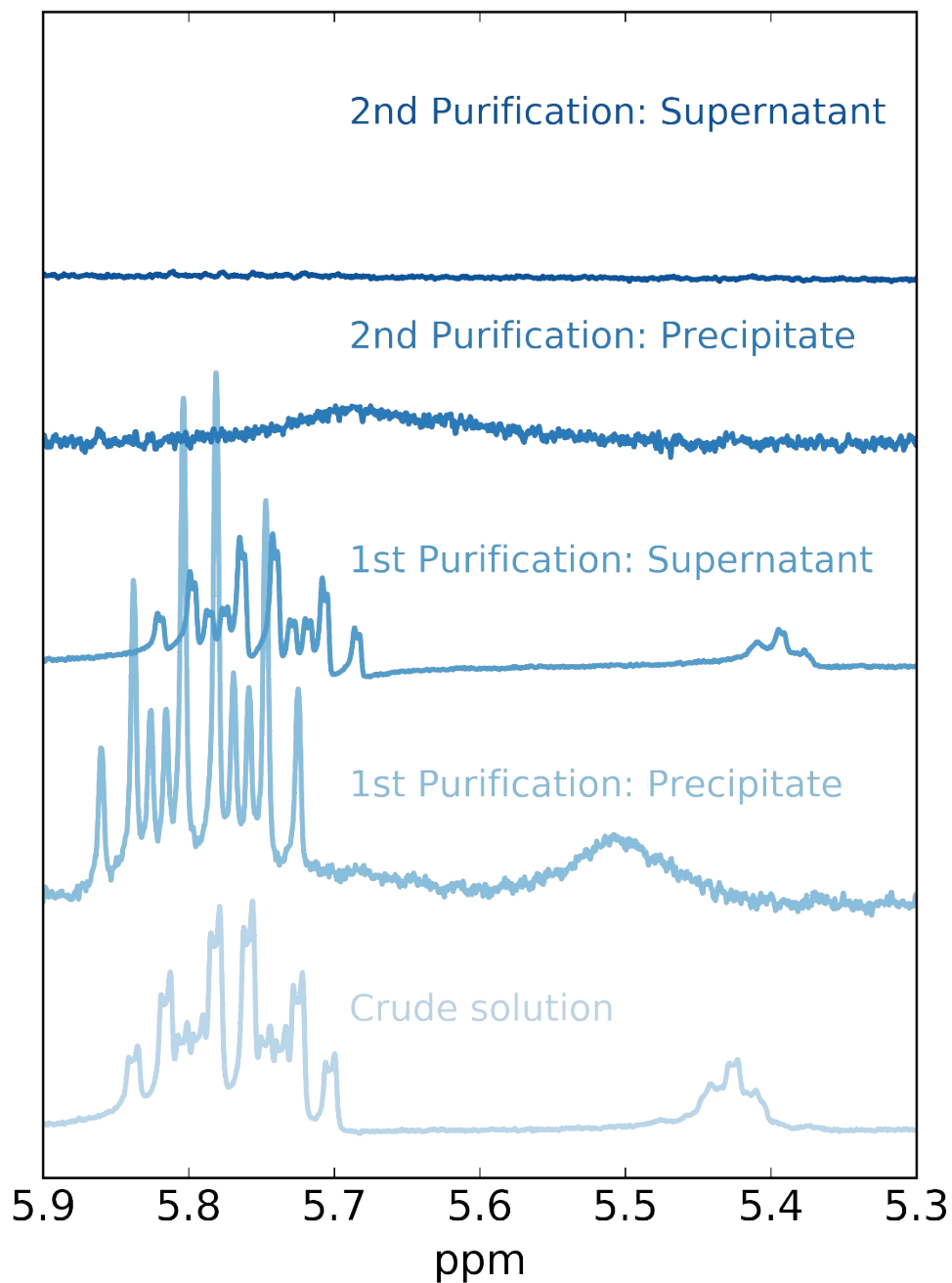


Figure S6: Following synthesis, NCs can be separated from the solvent, unreacted precursors, and free ligands using antisolvent precipitation with acetone.<sup>10</sup> The crude solution of product clearly demonstrates  $^1\text{H}$  resonances from ODE (5.9-5.7 ppm) and free oleic acid (5.55-5.4 ppm). Once the solution undergoes the first purification step, the precipitate shows signatures of ODE and a broadened oleic acid resonance, consistent with oleic acid bound to the NC surface.<sup>11</sup> By contrast, only free oleic acid and ODE is observed in the supernatant. A second purification step effectively separates the NCs from ODE, leaving only the broad bound oleic acid resonances. No signals are observed from the supernatant in this range, though these spectra are not quantitative as several dilutions and concentrations were performed.

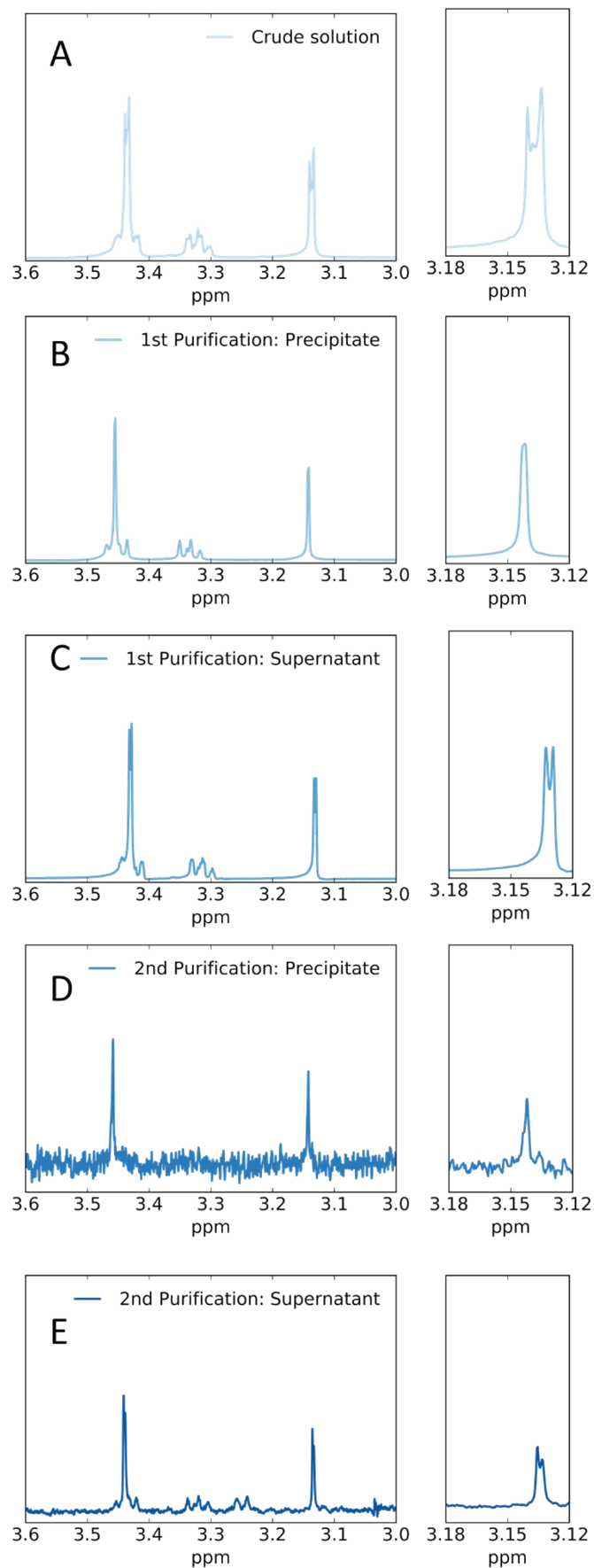


Figure S7: Partitioning of tetraglyme through purification as observed by  $^1\text{H}$  NMR. A) The crude solution exhibits the distinctly split tetraglyme resonance (c.f. Figure S3). In particular, the  $\text{CH}_3$  resonance near 3.13 ppm (highlighted in the right panels) is consistent with a mixture of split (coordinated) and single-peaked (uncoordinated) tetraglyme, similar to our observations in powders of lead oleate and tetraglyme (Figure S3). Further purification asymmetrically partitions the tetraglyme. The uncoordinated tetraglyme (single-peaked resonances similar to free tetraglyme (Figure S2)) fractionates to the precipitate (B,D) while the coordinated tetraglyme (double-peaked resonances as seen in Figure S3) remains in the supernatant (C, E). In contrast to oleic acid (Figure S6), no peak broadening is observed, consistent with the absence of bound tetraglyme on the surface on the NCs.

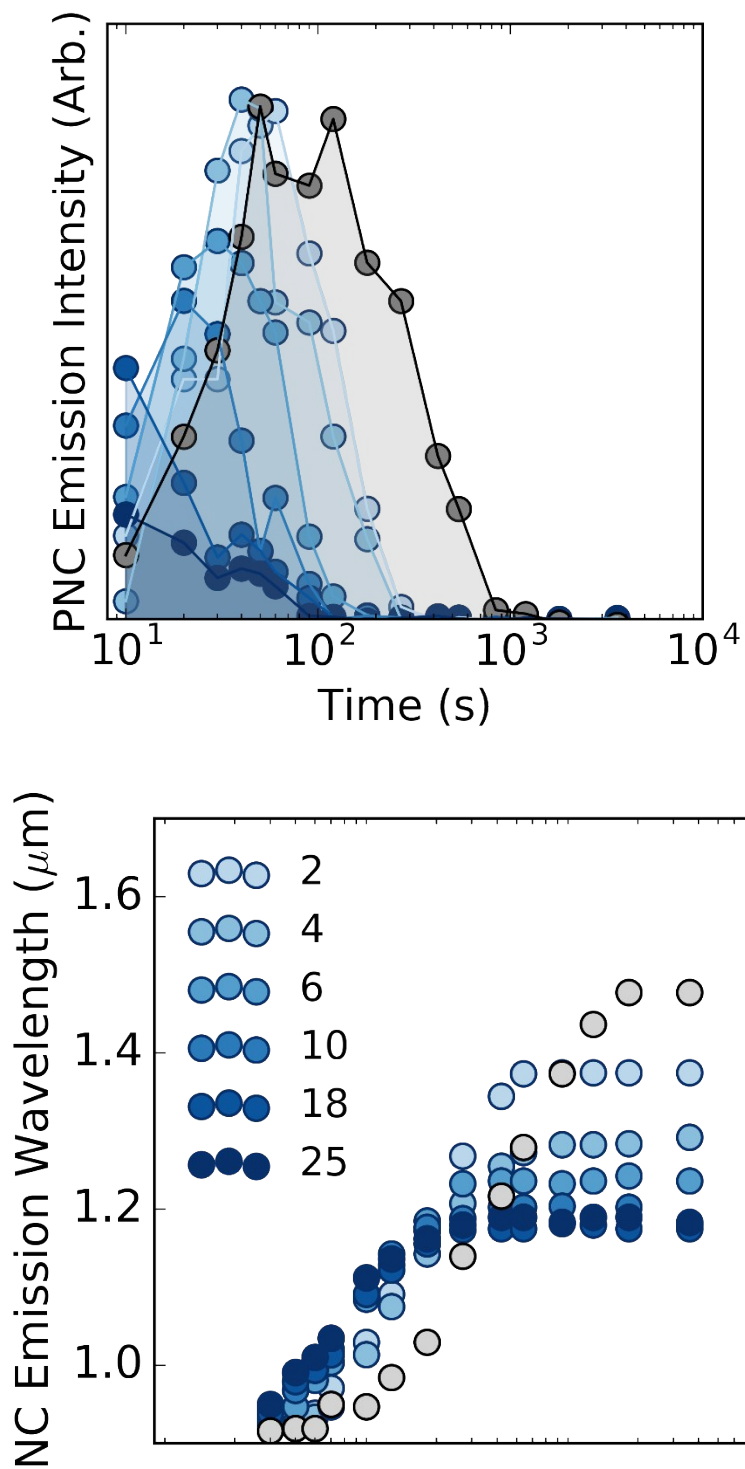


Figure S8: Effect of tetraglyme on the nucleation and growth of PbS nanocrystals. Gray circles indicate the reaction without tetraglyme, and the legend indicates the number of tetraglyme:Pb equivalents used. As tetraglyme is progressively added the data is colored from pale blue to dark blue. Top) PNC emission intensity over time with varying amounts of tetraglyme. Bottom) Position of the NC emission feature over time.

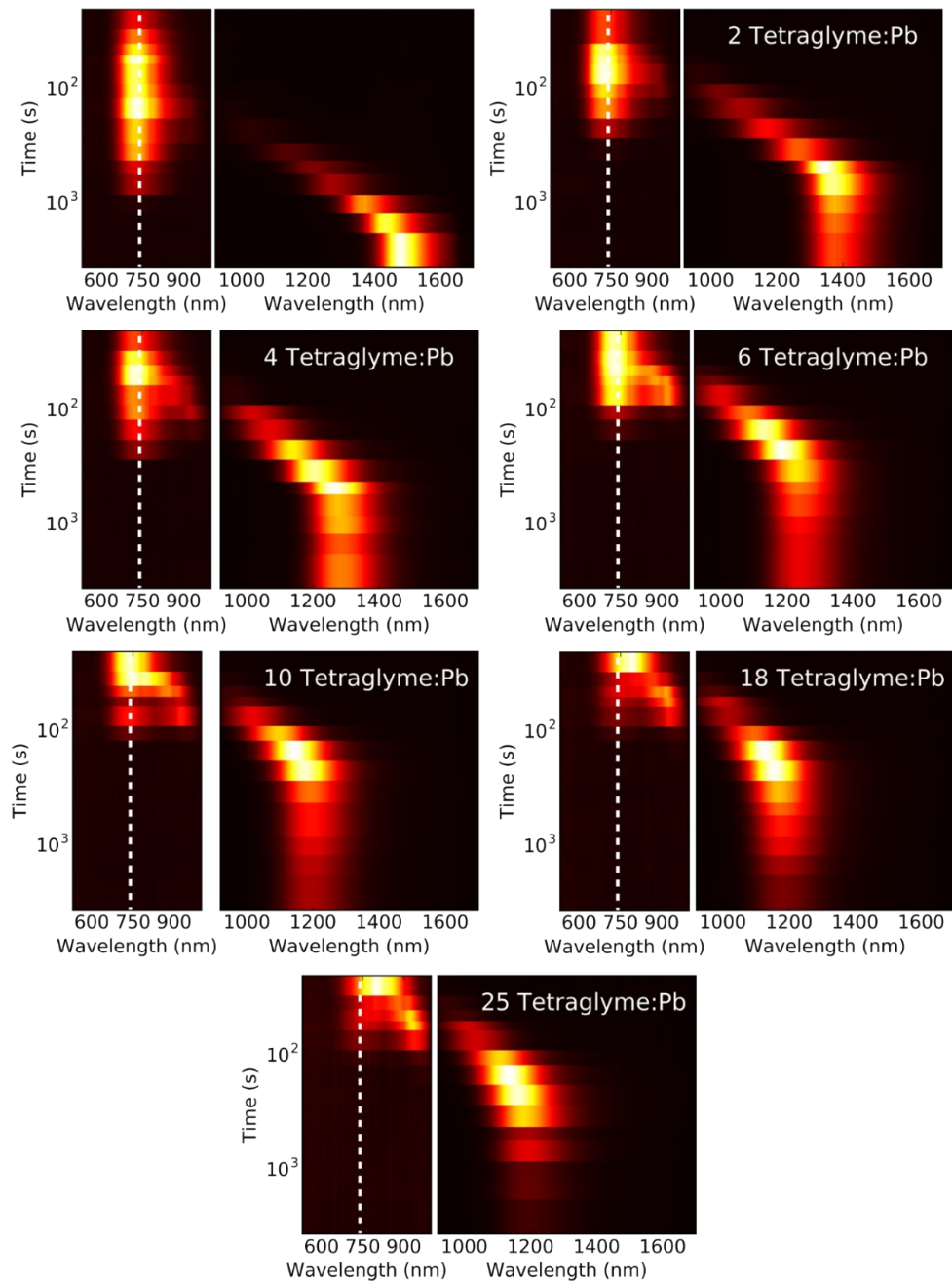


Figure S9: Dependence of the reaction kinetics on the tetraglyme concentration as monitored by the emission of aliquots taken periodically during synthesis of PbS NCs. All other synthetic conditions are as per our dilute reference reaction. (See Experimental Section for Methods) These data are from the same set of reactions that are summarized in Figures 2, 3 and S8.

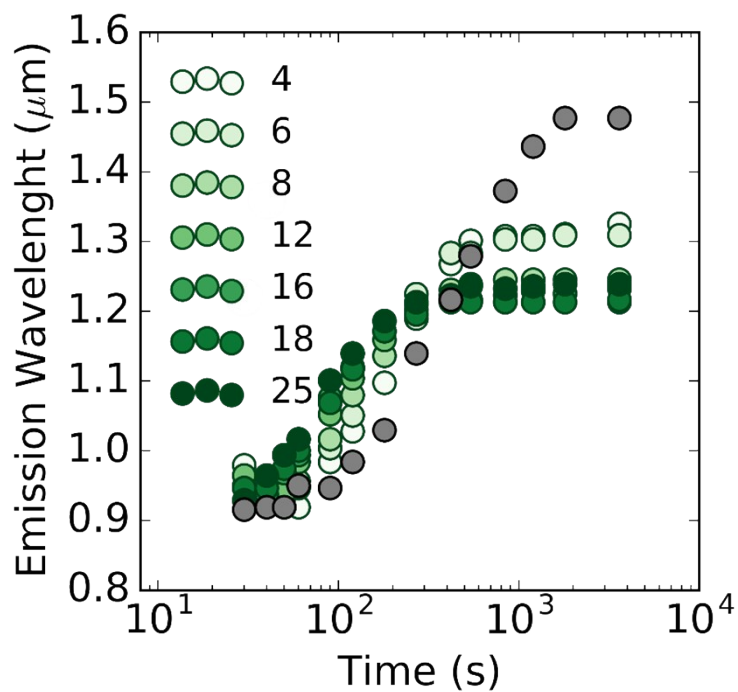
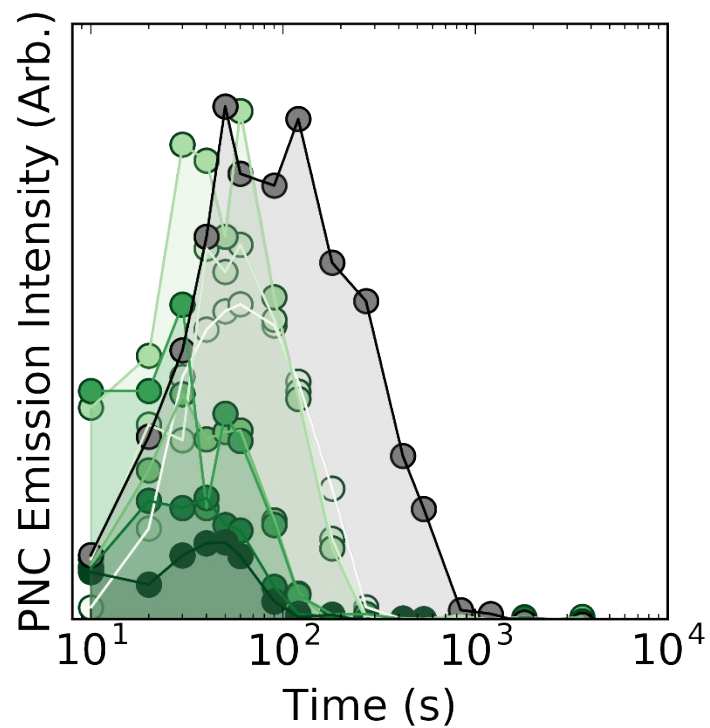


Figure S10: Effect of triglyme on the nucleation and growth of PbS nanocrystals. Gray circles indicate the reaction without triglyme, and the legend indicates the number of triglyme:Pb equivalents used. As triglyme is progressively added the data is colored from pale green to dark green. Top) PNC emission intensity over time with varying amounts of triglyme. Bottom) Position of the NC emission feature over time

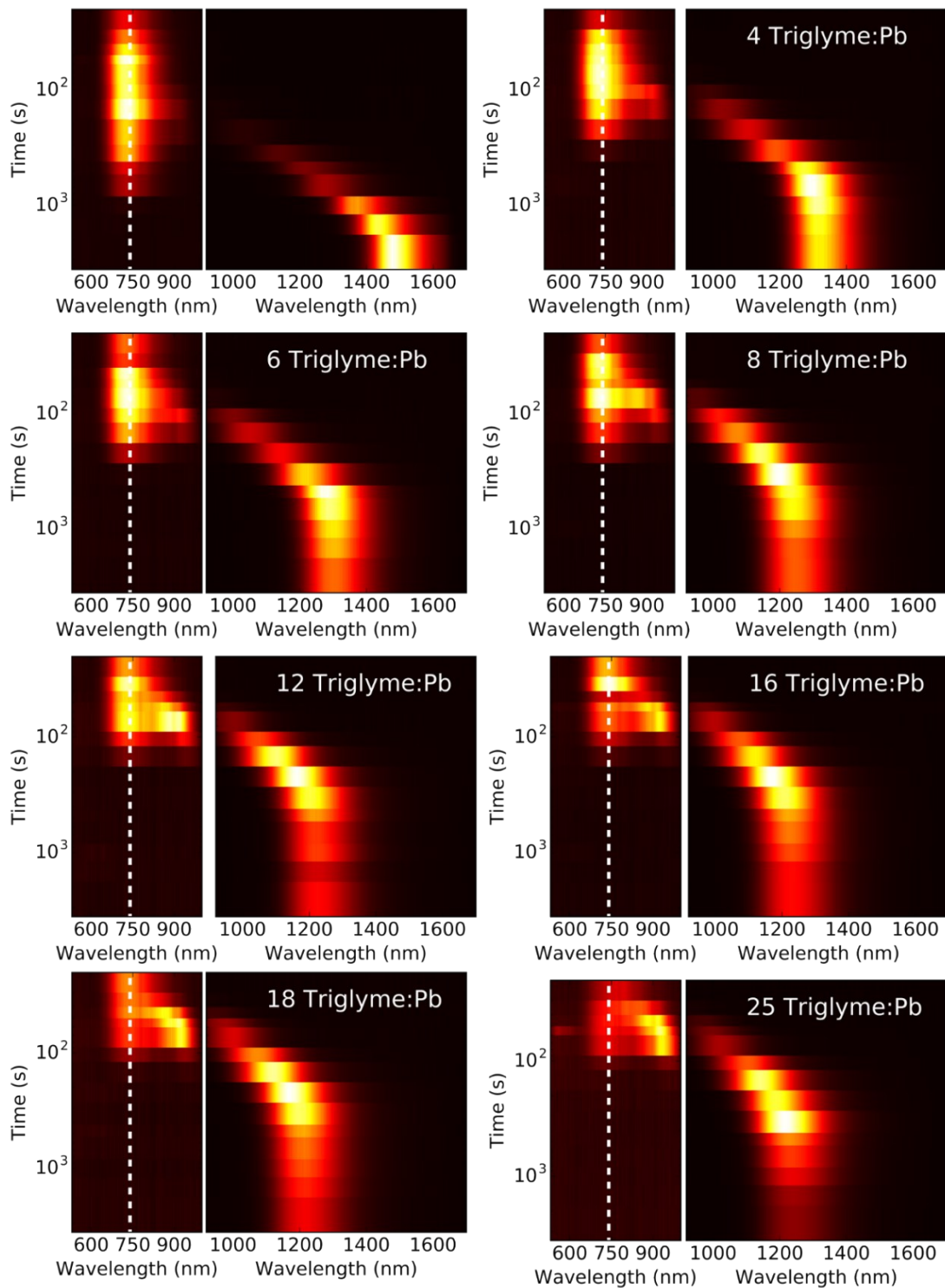


Figure S11: Dependence of the reaction kinetics on the triglyme concentration as monitored by the emission of aliquots taken periodically during synthesis of PbS NCs. All other synthetic conditions are as per our dilute reference reaction. (See Experimental Section for Methods) These data are from the same set of reactions that are summarized in Figures 3 and S10.

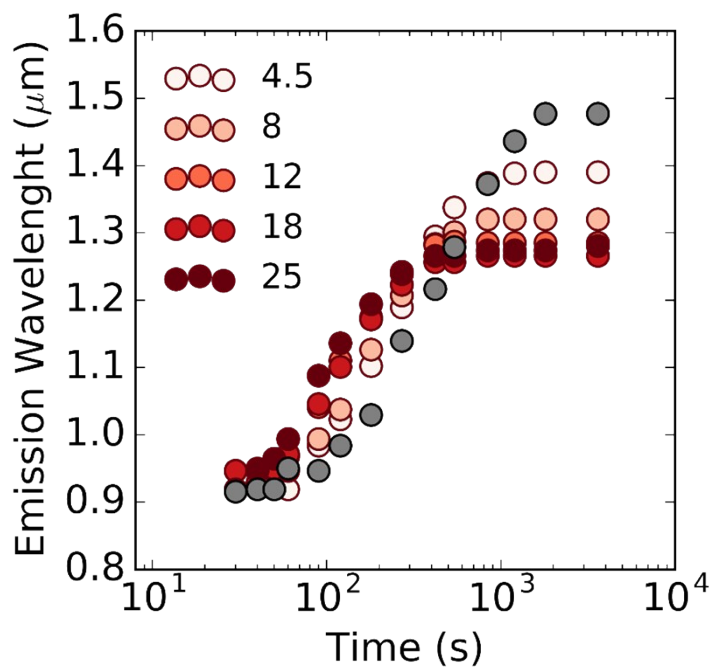
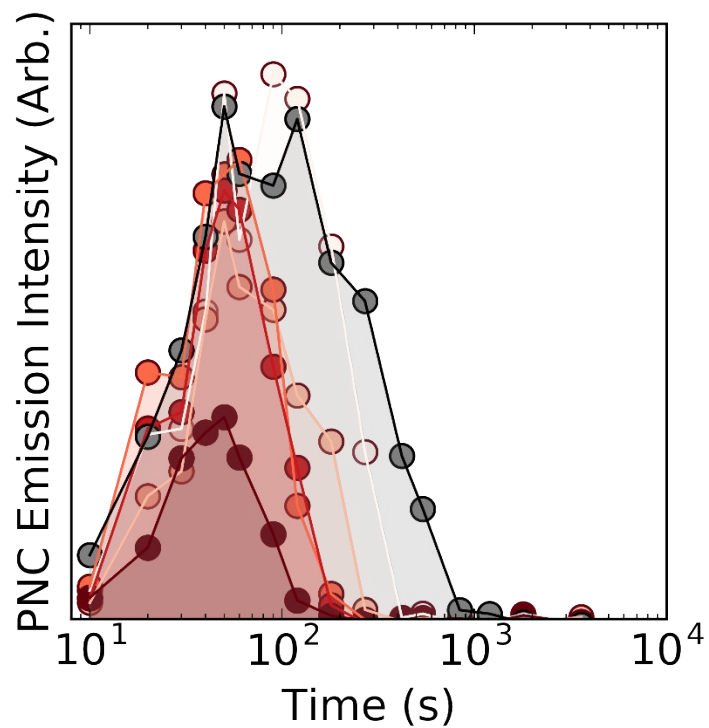


Figure S12: Effect of diglyme on the nucleation and growth of PbS nanocrystals. Gray circles indicate the reaction without diglyme, and the legend indicates the number of diglyme:Pb equivalents used, coloured from pale to dark red as diglyme is progressively added. Top) PNC emission intensity over time with varying amounts of diglyme. Bottom) Position of the NC emission feature over time.

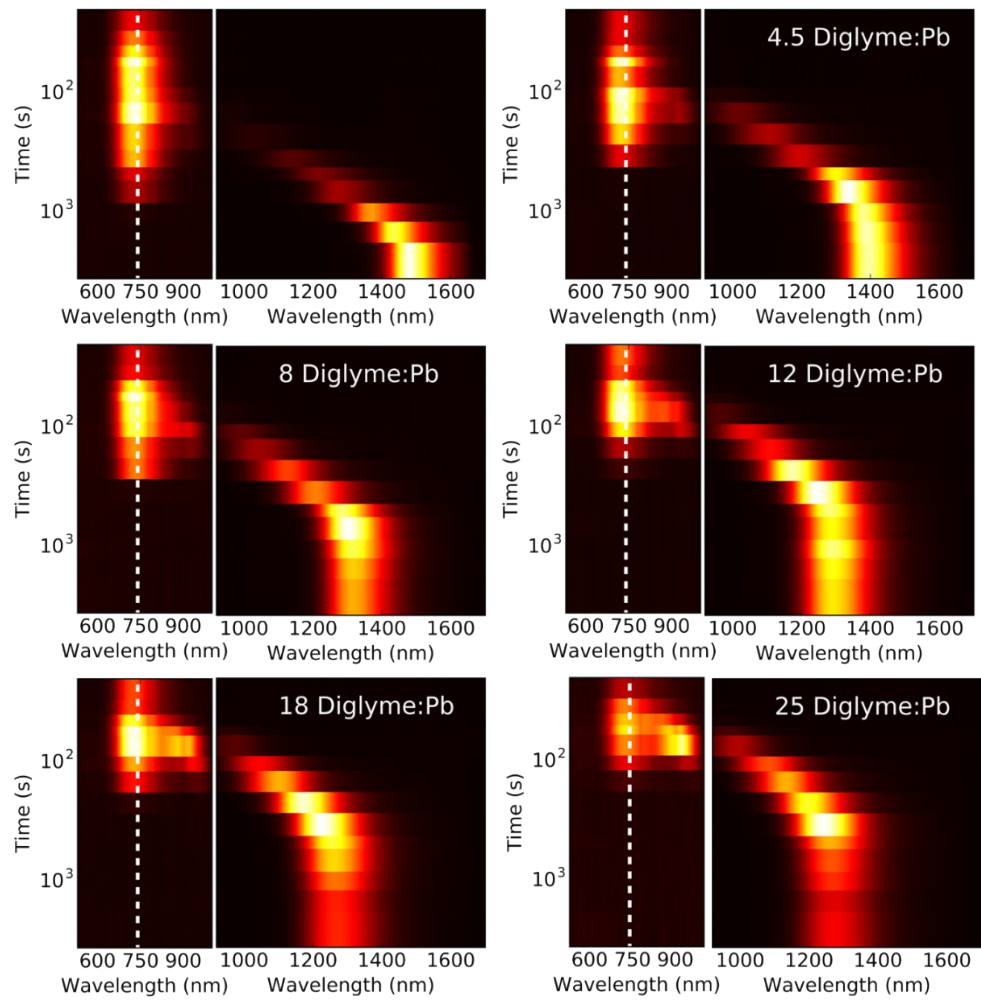


Figure S13: Dependence of the reaction kinetics on the diglyme concentration as monitored by the emission of aliquots taken periodically during synthesis of PbS NCs. All other synthetic conditions are as per our dilute reference reaction. (See Experimental Section for Methods) These data are from the same set of reactions that are summarized in Figures 3 and S12.

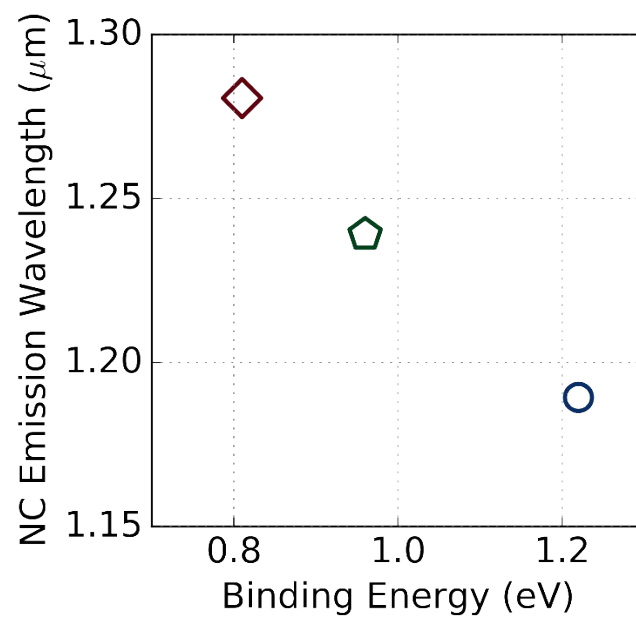


Figure S14: Final size at reaction completion for reactions including 25:1 glyme:Pb. (Red diamond: Diglyme, Green pentagon: Triglyme, Blue circle: Tetraglyme)

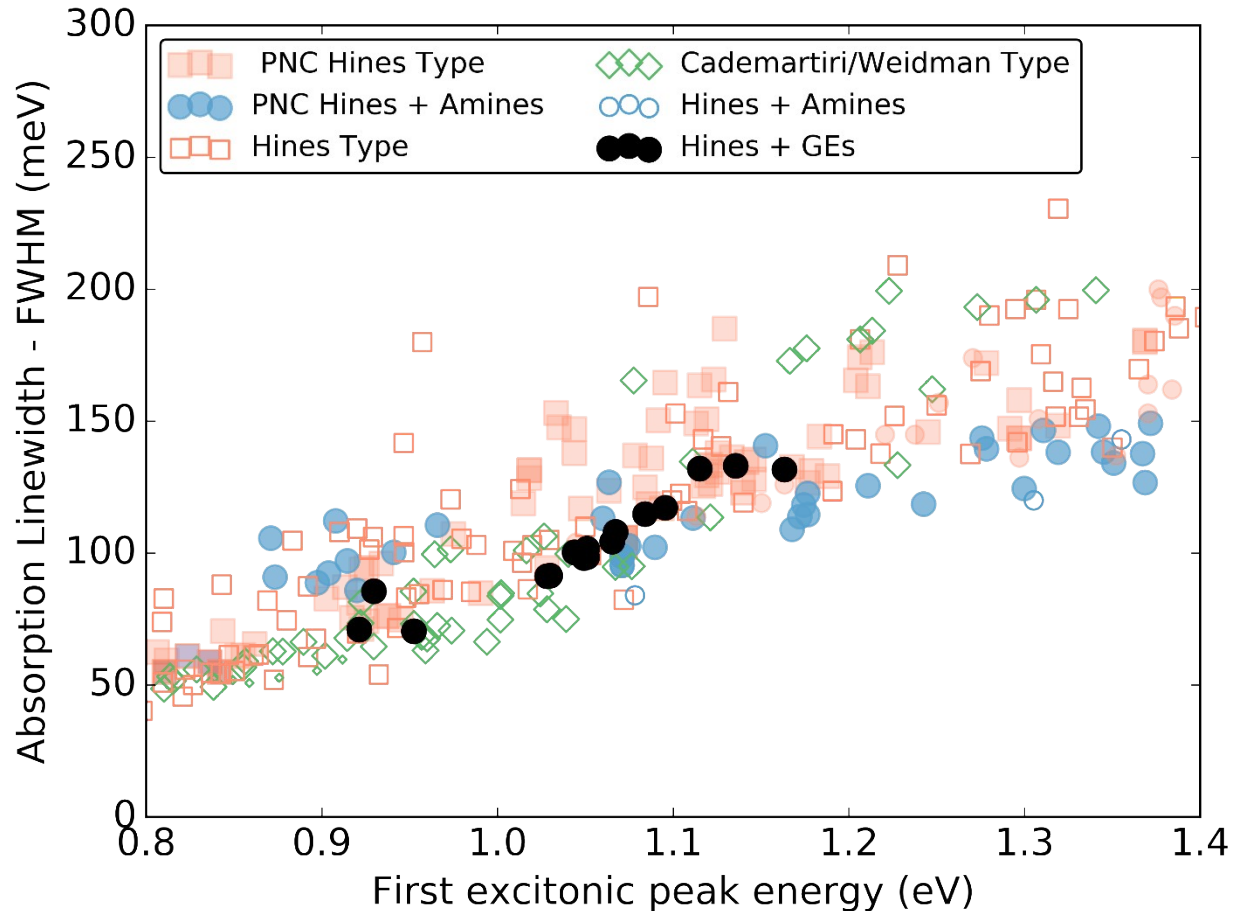


Figure S15: Absorption linewidths of NCs prepared with glycol ethers (GEs, black circles) compared to other synthetic routes. Highlighted are the NCs where the PNC kinetics were targeted to control size and dispersity such as the filled red squares involving the classical route and filled blue circles which involved amines.<sup>1</sup> Empty red squares, green diamonds and blue circles are literature values found for the classical Hines approach, the Cademartiri/Weidman approach and the Hines with amines approach.<sup>2,3,8,9,12-27</sup>

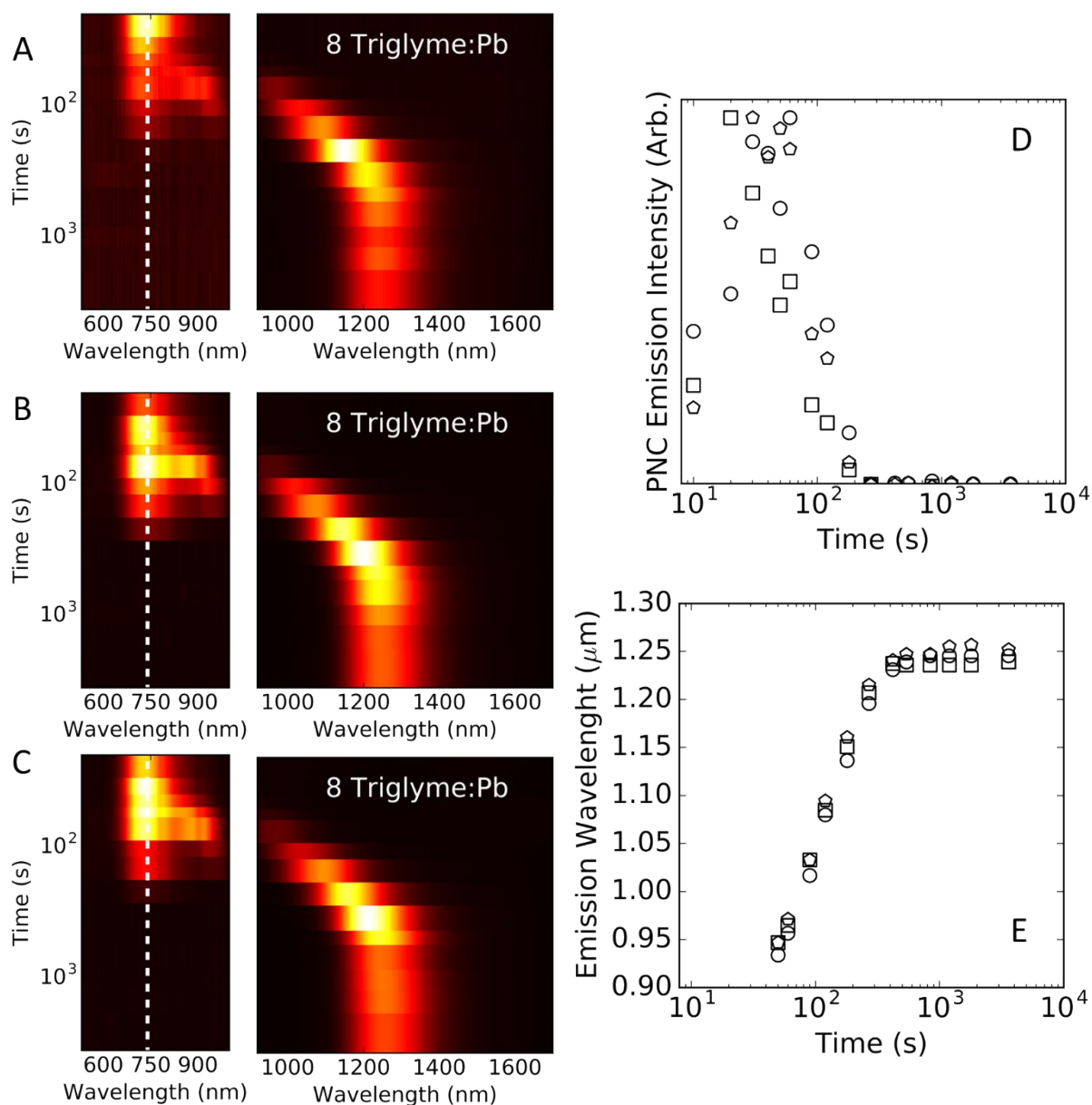


Figure S16: Reproducibility of reactions performed with 8:1 triglyme:Pb. Panels A to C show the fluorescence from aliquots taken periodically from three different reactions performed using the same conditions. The spectral evolution of PNC and NCs are very similar from batch to batch. Panels D summarizes the extracted PNC emission intensities (normalized to the maximum of each reaction) over time, while Panel E similarly tracks the peak NC emission wavelength through each reaction. The three batches demonstrate reproducible kinetics and a consistent final NC size. The standard error of the final peak emission wavelength is calculated to be 5 nm.

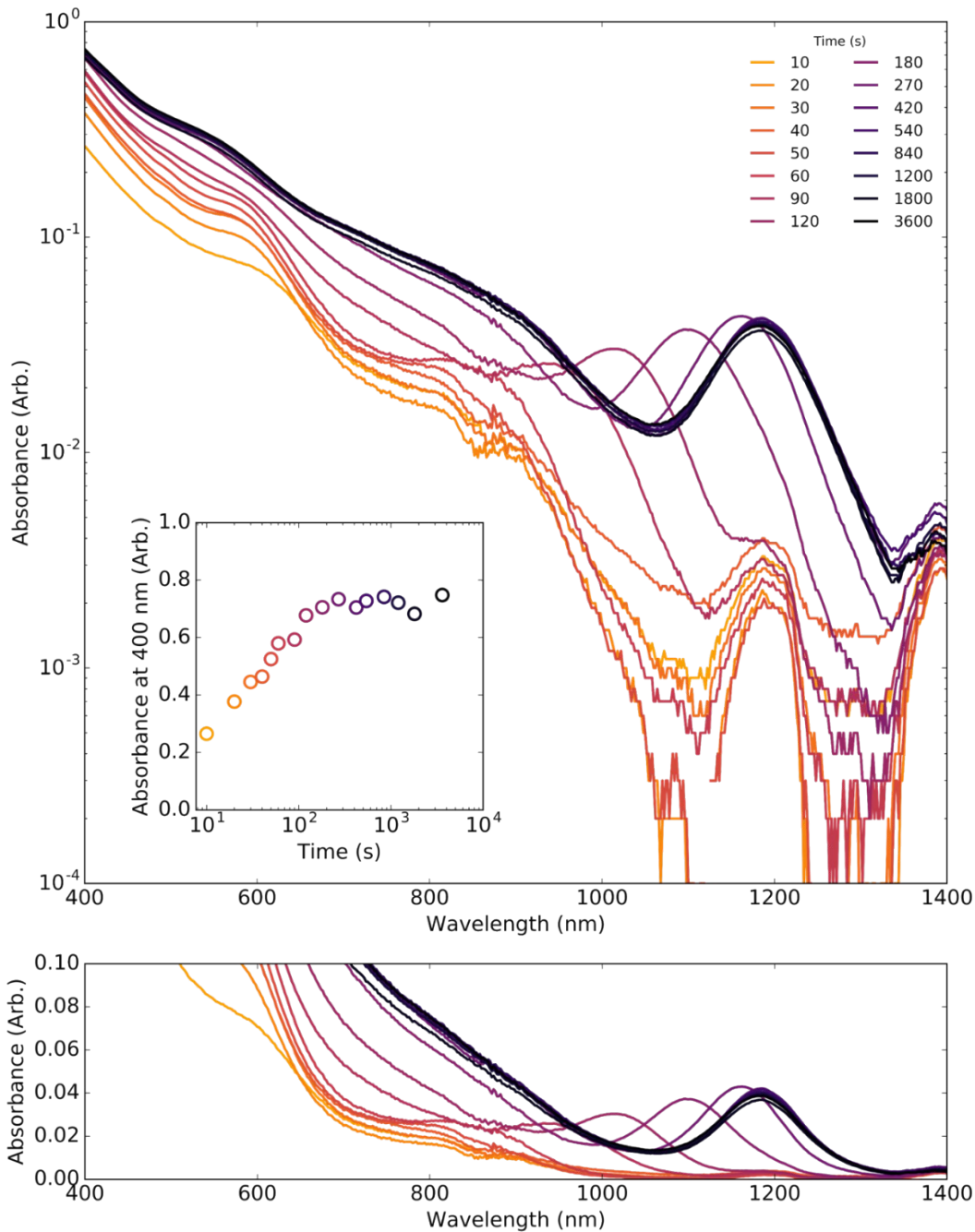


Figure S17: Using absorption spectra to track the progress of a reaction with 8:1 triglyme:Pb. The top panel (logarithmic intensity) shows the delayed appearance of NCs (excitonic absorption peaks near 800 nm in this reaction) compared to the early formation of PNCs (absorption peak near 600 nm in early spectra). The bottom panel presents the same data on a linear scale. The weak features near 1200 nm and 1400 nm are due to the solvent. The evolution of the NC excitonic absorption peak asymptotes beyond  $\sim 1000$ s, consistent with reaction completion (See above) The inset figure tracks the absorption at 400 nm using the same colour scale, showing that it saturates over the same time scale. Comparing to the fluorescence from this reaction (Figure S16, panel C) this asymptotic behaviour also temporally aligns with the emission spectrum.

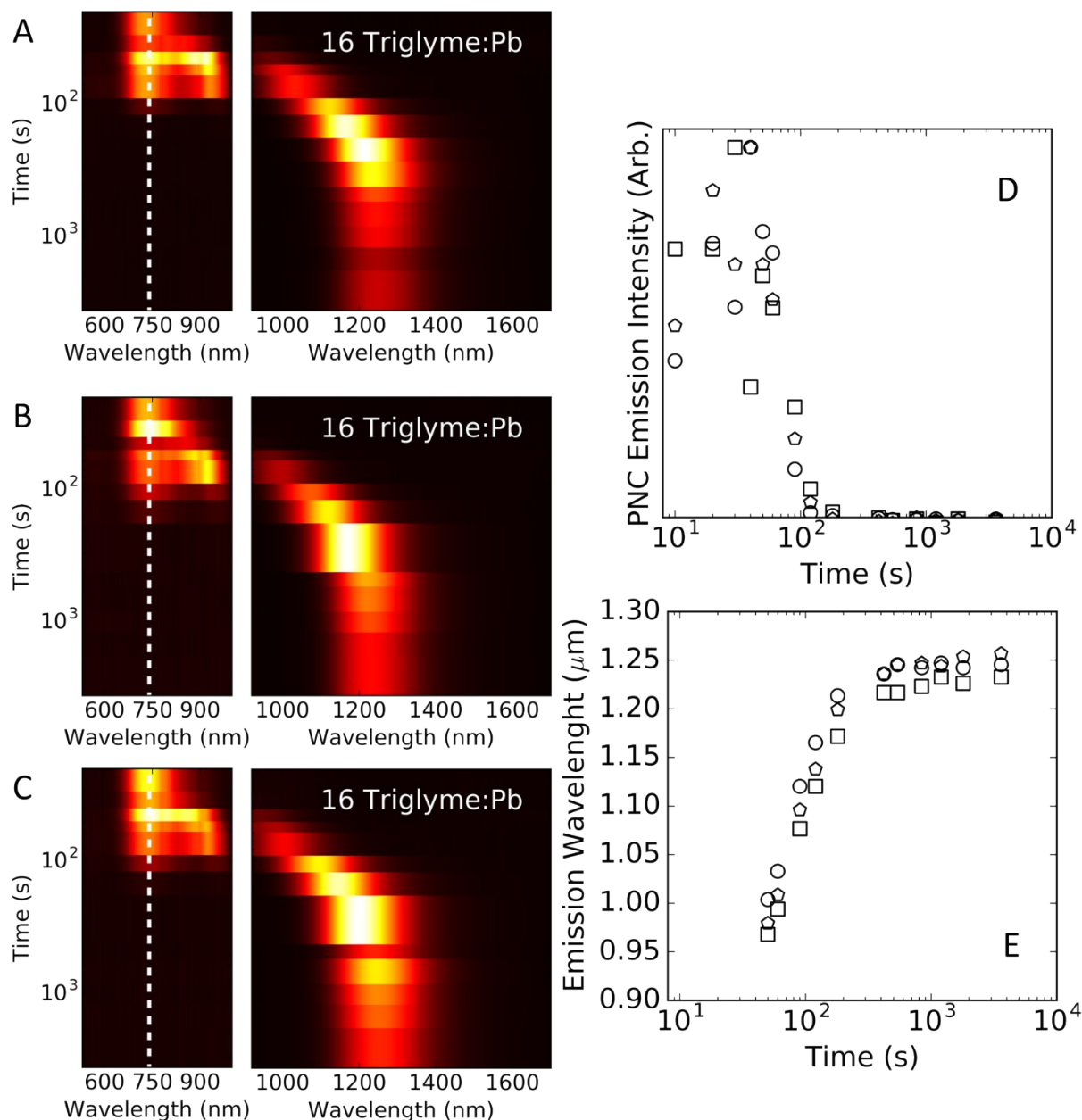


Figure S18: Reproducibility of reactions performed with 16:1 triglyme:Pb. Panels A to C show the fluorescence from aliquots taken periodically from three different reactions performed using the same conditions. The spectral evolution of PNC and NCs are very similar from batch to batch. Panels D summarizes the extracted PNC emission intensities (normalized to the maximum of each reaction) over time, while Panel E similarly tracks the peak NC emission wavelength through each reaction. The three batches demonstrate reproducible kinetics and a consistent final NC size. The standard error of the final peak emission wavelength is calculated to be 11 nm. This value was used to produce the error bars in Figure 3 of the main manuscript.

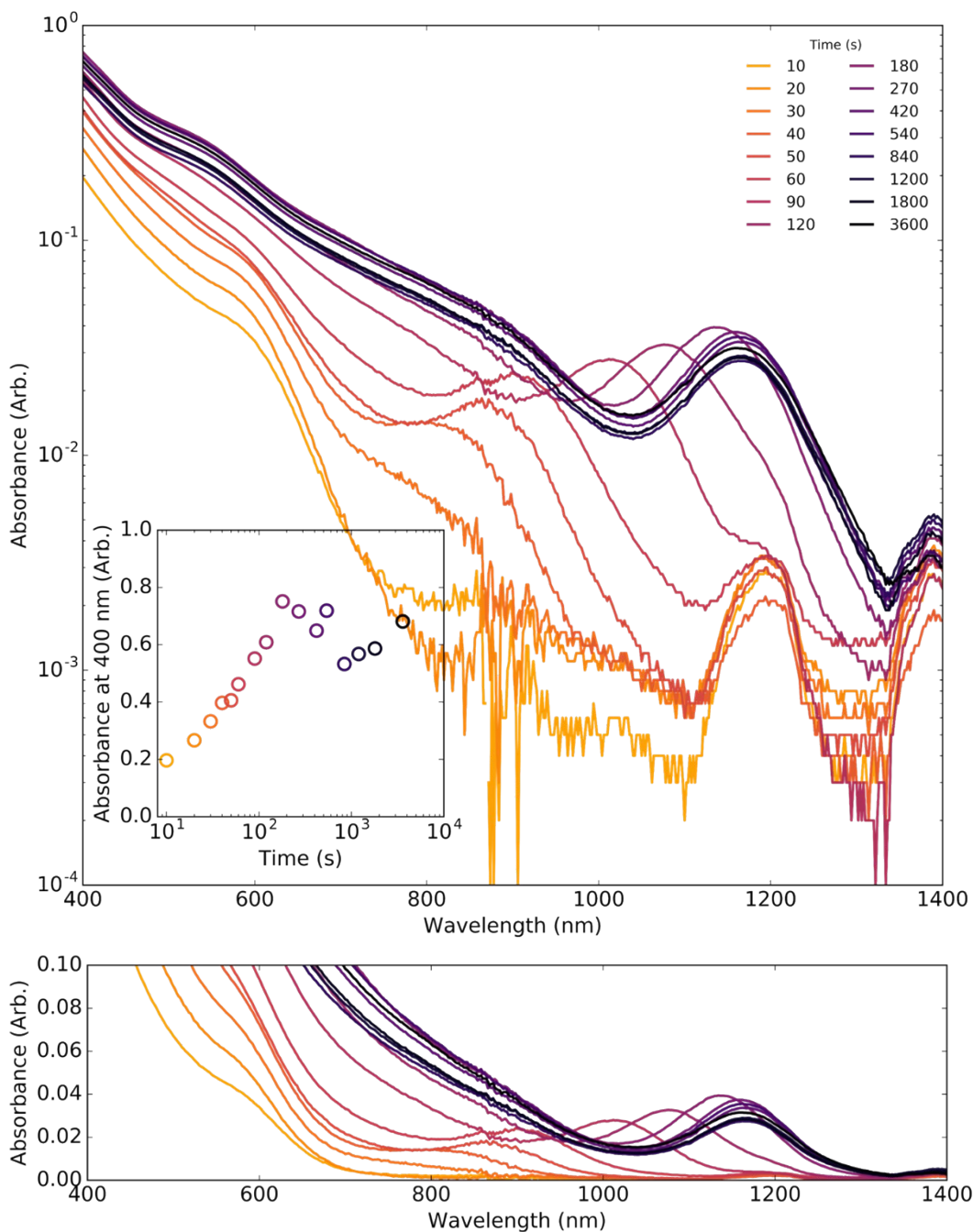


Figure S19: *Using absorption spectra to track the progress of a reaction with 16:1 triglyme:Pb.* The top panel (logarithmic intensity) shows the delayed appearance of NCs (excitonic absorption peaks between 800–1000 nm in this reaction) compared to the early formation of PNCs (absorption peak near 600nm in early spectra). The bottom panel presents the same data on a linear scale. The weak features near 1200 nm and 1400 nm are due to the solvent. The evolution of the NC excitonic absorption peak asymptotes beyond  $\sim 500$ s, consistent with reaction completion (See above) The inset figure tracks the absorption at 400 nm using the same colour scale, showing that it saturates over the same time scale. Comparing to the fluorescence from this reaction (Figure S18, Panel C) this asymptotic behaviour also temporally aligns with the emission spectrum.

## References:

- 1 P. B. Green, P. Narayanan, Z. Li, P. Sohn, C. J. Imperiale and M. W. B. Wilson, *Chem. Mater.*, 2020, **32**, 4083–4094.
- 2 J. W. Lee, D. Y. Kim, S. Baek, H. Yu and F. So, *Small*, 2016, **12**, 1246–1246.
- 3 M. Hines and G. D. Scholes, *Adv. Mater.*, 2003, **15**, 1844–1849.
- 4 Y. Zhang, T. D. Siegler, C. J. Thomas, M. K. Abney, T. Shah, A. De Gorostiza, R. M. Greene and B. A. Korgel, *Chem. Mater.*, 2020, acs.chemmater.0c01735.
- 5 I. Moreels, K. Lambert, D. Smeets, D. De Muynck, T. Nollet, C. Martins, F. Vanhaecke, C. Delerue, G. Allan and Z. Hens, *ACS Nano*, 2009, **3**, 3023–3030.
- 6 X. Peng, J. Wickham and A. P. Alivisatos, *J. Am. Chem. Soc.*, 1998, **120**, 5343–5344.
- 7 S. Abe, R. K. Čapek, B. De Geyter and Z. Hens, *ACS Nano*, 2012, **6**, 42–53.
- 8 M. P. Hendricks, M. P. Campos, G. T. Cleveland, I. Jen-La Plante and J. S. Owen, *Science*, 2015, **348**, 1226–1230.
- 9 O. Voznyy, L. Levina, J. Z. Fan, M. Askerka, A. Jain, M. Choi, O. Ouellette, P. Todorović, L. K. Sagar and E. H. Sargent, *ACS Nano*, 2019, **13**, 11122–11128.
- 10 C. B. Murray, C. R. Kagan and M. G. Bawendi, *Annu. Rev. Mater. Sci.*, 2000, 545–610.
- 11 Z. Hens and J. C. Martins, *Chem. Mater.*, 2013, **25**, 1211–1221.
- 12 I. Moreels, Y. Justo, B. De Geyter, K. Haustraete, J. C. Martins and Z. Hens, *ACS Nano*, 2011, **5**, 2004–2012.
- 13 L. Cademartiri, J. Bertolotti, R. Sapienza, D. S. Wiersma, G. von Freymann and G. A. Ozin, *J. Phys. Chem. B*, 2006, **110**, 671–673.
- 14 C. C. Reinhart and E. Johansson, *Chem. Mater.*, 2015, **27**, 7313–7320.
- 15 J. J. Peterson and T. D. Krauss, *Nano Lett.*, 2006, **6**, 510–514.
- 16 Z. Huang, Z. Xu, M. Mahboub, Z. Liang, P. Jaimes, P. Xia, K. R. Graham, M. L. Tang and T. Lian, *J. Am. Chem. Soc.*, 2019, **141**, 9769–9772.
- 17 O. Voznyy, L. Levina, F. Fan, G. Walters, J. Z. Fan, A. Kiani, A. H. Ip, S. M. Thon, A. H. Proppe, M. Liu and E. H. Sargent, *Nano Lett.*, 2017, **17**, 7191–7195.
- 18 J. R. Caram, S. N. Bertram, H. Utzat, W. R. Hess, J. A. Carr, T. S. Bischof, A. P. Beyler, M. W. B. Wilson and M. G. Bawendi, *Nano Lett.*, 2016, **16**, 6070–6077.
- 19 A. Shrestha, N. A. Spooner, S. Z. Qiao and S. Dai, *Phys. Chem. Chem. Phys.*, 2016, **18**, 14055–14062.
- 20 M. C. Weidman, M. E. Beck, R. S. Hoffman, F. Prins and W. A. Tisdale, *ACS Nano*, 2014, 6363–6371.
- 21 A. Preske, J. Liu, O. V. Prezhdo and T. D. Krauss, *ChemPhysChem*, 2016, **17**, 681–686.
- 22 L. Nienhaus, M. Wu, N. Geva, J. J. Shepherd, M. W. B. Wilson, V. Bulovic, T. Van Voorhis, M. A. Baldo and M. G. Bawendi, *ACS Nano*, 2017, **11**, 7848–7857.

- 23 B. Hou, Y. Cho, B. S. Kim, J. Hong, J. B. Park, S. J. Ahn, J. I. Sohn, S. Cha and J. M. Kim, *ACS Energy Lett.*, 2016, **1**, 834–839.
- 24 M. Yarema, O. Yarema, W. M. M. Lin, S. Volk, N. Yazdani, D. Bozyigit and V. Wood, *Chem. Mater.*, 2017, **29**, 796–803.
- 25 J. Maes, N. Castro, K. De Nolf, W. Walravens, B. Abécassis and Z. Hens, *Chem. Mater.*, 2018, **30**, 3952–3962.
- 26 R. H. Gilmore, E. M. Y. Lee, M. C. Weidman, A. P. Willard and W. A. Tisdale, *Nano Lett.*, 2017, **17**, 893–901.
- 27 M. C. Weidman, D. M. Smilgies and W. A. Tisdale, *Nat. Mater.*, 2016, **15**, 775–781.